

See discussions, stats, and author profiles for this publication at: <https://www.researchgate.net/publication/270656133>

Diversity of acoustic streaming in a rectangular acoustofluidic field

Article in *Ultrasonics* · December 2014

DOI: 10.1016/j.ultras.2014.11.015 · Source: PubMed

CITATIONS

48

READS

1,477

2 authors:



Qiang Tang

Huaiyin Institute of Technology

27 PUBLICATIONS 170 CITATIONS

[SEE PROFILE](#)



Junhui Hu

Nanyang Technological University

160 PUBLICATIONS 1,955 CITATIONS

[SEE PROFILE](#)

Some of the authors of this publication are also working on these related projects:



This work was supported by the following funding organizations in China: the National Natural Science Foundation of China (Grant No. 11904117), the Industry-University-Research Collaboration Project of Jiangsu Province (Grant No. BY2019058), the Scientific Research Foundation of Huaiyin Institute of Technology (Grant No. Z301B19529), and the Training Foundation of Postgraduate Supervisor (Grant No. Z206E20555). Dr Qiang Tang thanks the Jiangsu Government Scholarship for Overseas Studies. [View project](#)



gas identification [View project](#)



Diversity of acoustic streaming in a rectangular acoustofluidic field



Qiang Tang, Junhui Hu*

State Key Lab of Mechanics and Control of Mechanical Structures, Nanjing University of Aeronautics and Astronautics, Nanjing 210016, China

ARTICLE INFO

Article history:

Received 26 February 2014
Received in revised form 24 November 2014
Accepted 25 November 2014
Available online 10 December 2014

Keywords:

Acoustic streaming
Diversity

ABSTRACT

Diversity of acoustic streaming field in a 2D rectangular chamber with a traveling wave and using water as the acoustic medium is numerically investigated by the finite element method. It is found that the working frequency, the vibration excitation source length, and the distance and phase difference between two separated symmetric vibration excitation sources can cause the diversity in the acoustic streaming pattern. It is also found that a small object in the acoustic field results in an additional eddy, and affects the eddy size in the acoustic streaming field. In addition, the computation results show that with an increase of the acoustic medium's temperature, the speed of the main acoustic streaming decreases first and then increases, and the angular velocity of the corner eddies increases monotonously, which can be clearly explained by the change of the acoustic dissipation factor and shearing viscosity of the acoustic medium with temperature. Commercialized FEM software COMSOL Multiphysics is used to implement the computation tasks, which makes our method very easy to use. And the computation method is partially verified by an established analytical solution.

© 2014 Elsevier B.V. All rights reserved.

1. Introduction

Acoustic streaming is a kind of macroscopic flow caused by a sound field, which exists in viscous fluid [1–4]. It is well known that a sound wave in fluid can drive material points of fluid to vibrate near its equilibrium position back and forth. When the strength of a sound wave is proper, a time-independent flow will be generated in the sound field, which is so called acoustic streaming. Eckhart streaming is an important acoustic streaming, which is caused by the acoustic absorption in a sound field [4]. At the present stage, it is the major means which the ultrasonic nano manipulation technology is using [24].

The conventional applications of acoustic streaming are in ultrasonic cleaning [5], dispersion [5], mixing [6], non-contact driving [7,24], etc. In ultrasonic manipulations, the acoustic streaming is usually a negative factor because it will flush away micro particles trapped by the acoustic radiation force [8,9]. Recently, the authors' research team demonstrated that the acoustic streaming is a very useful means to manipulate nano objects [10–13]. The mobile acoustic streaming field, generated by a micro vibrating rod, can be used to suck, orientate, position and trap individual nanowires in a noncontact and contact way [10,11], and to rotary drive a single nanowire in water on a substrate [12]. The acoustic streaming field in a droplet on an ultrasonic stage can also

be used to concentrate nano objects in a controlled way [13]. For better and wider applications of acoustic streaming in nano manipulation, present understandings of acoustic streaming are far from being sufficient, and more investigation of acoustic streaming, is needed for the design of practical devices for nano manipulations.

Numerical calculation is an effective way to make us understand the acoustic streaming more thoroughly. Eckhart streaming can be calculated by the Navier–Stokes equation, continuity equation and boundary conditions [14–16]. Kamakura's group calculated the acoustic streaming generated by a Gaussian beam [17] and analyzed the transient process of acoustic streaming from a planar ultrasound source [18]. Nakamura's group calculated the acoustic streaming in an acoustic air pump by the finite element method (FEM), in which the acoustic field is viewed as a fluidic field, the acoustic streaming velocity is obtained by filtering away the vibration component in the total fluidic velocity [19]. In the research and development of practical devices, more convenient and efficient numerical methods are needed to calculate the Eckhart streaming field in the devices and to analyze its change with the working and structural parameters of devices.

In this work, steady acoustic streaming in a 2D rectangular chamber with a traveling wave and using water as acoustic medium is computed and analyzed by the FEM, and the results reveal a diversity in the acoustic streaming field's pattern, which was taken little notice before this work. Our results show that the diversity in the acoustic streaming field's pattern can be caused by the working frequency, the vibration excitation source length,

* Corresponding author.

E-mail address: ejhhu@nuaa.edu.cn (J. Hu).

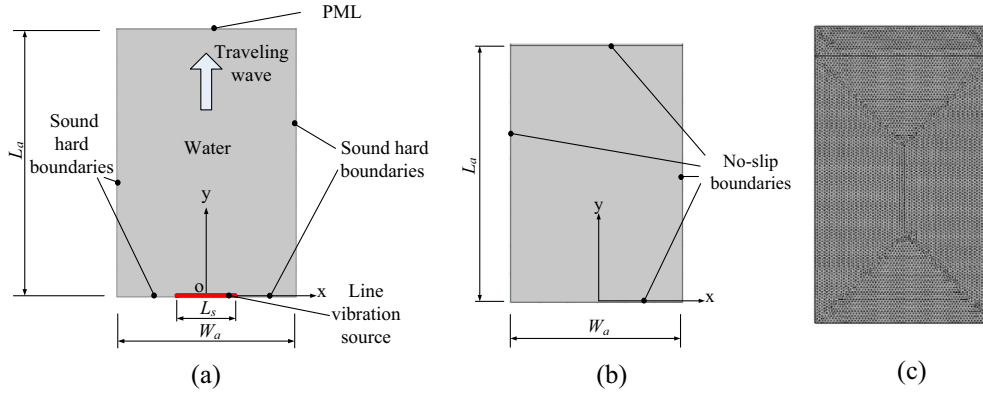


Fig. 1. Model and mesh of the acoustofluidic field. (a) Computation model for the sound field. (b) Boundary conditions of the acoustic streaming field. (c) Mesh of the acoustofluidic field.

the distance and phase difference between two separated symmetric vibration excitation sources, and the existence of a small object in the acoustic field. In addition, the effects of the temperature of the acoustic medium on the acoustic streaming field's pattern and velocity are clarified theoretically and explained.

2. Calculation method and conditions

Our computation of acoustic streaming is implemented by the FEM software COMSOL Multiphysics. The computation process consists of three steps. In the first step, the sound field is solved first by the acoustic module of the software. In the second step, vibration velocity and sound pressure of the sound field are used to calculate spatial gradients of the Reynolds stress and mean pressure by the post processing functions of the software, which generate the acoustic streaming. In the last step, the steady acoustic streaming is solved by the fluidic dynamics module, with proper boundary conditions for the acoustic streaming.

A computation model for the acoustofluidic field is shown in Fig. 1. The acoustofluidic field for the computation is rectangular and 2-dimensional. Water is used as the acoustic medium. In Fig. 1a, the vibration source (red¹ line) is on the fixed wall at $y = 0$. To generate a traveling wave in the field, the boundary opposite to the vibration source allows the sound wave to pass without any reflection and absorption, that is, a perfect matching layer (PML) is used to generate the traveling wave. The other boundaries of the sound field are acoustically hard ($\frac{\partial p}{\partial n} = 0$, where \mathbf{n} denotes the unit normal vector of the boundaries, see Fig. 1(a)). For the acoustic streaming field, all the boundaries are no-slip (see Fig. 1(b)). This is because our work is mainly interested in the overall pattern of acoustic streaming in the chamber, rather than the details of acoustic streaming near the boundaries. Fig. 1(c) shows a meshed model for the acoustofluidic field with the maximum element size of 0.001 m, which is about 1/75 of the wavelength of the sound field at 20 kHz ($\lambda = \frac{c}{f} \approx \frac{1500}{20} \text{ mm} = 75 \text{ mm}$). Unless otherwise specified, the dimensions and acoustic medium (water) properties shown in Table 1 [20] and Appendix A are used.

The following wave equation [21] is used to solve the sound field:

$$\rho \frac{\partial^2 p}{\partial t^2} = \rho c^2 \nabla^2 p + b \nabla \frac{\partial p}{\partial t} \quad (1)$$

where p is the sound pressure, ρ is the fluid density, c is the sound speed. And the acoustic dissipation factor b is calculated by

$$b = \frac{4}{3} \eta + \eta' + \kappa_t \left(\frac{1}{C_v} - \frac{1}{C_p} \right) \quad (2)$$

where η and η' are the shear and bulk coefficient of viscosity, κ_t is the thermal conductivity of the medium, and C_p and C_v are the heat capacities of the medium at constant pressure and volume, respectively.

The thermodynamic relation among pressure p , temperature T , and density ρ in a sound field can be written as [25]:

$$d\rho/\rho = \gamma \beta_T dp - \alpha_p dT \quad (3)$$

where γ is the specific heat ratio, β_T is the isothermal compressibility, and α_p is the isobaric thermal expansion coefficient. The values of γ , β_T , and α_p of water at 298 K are listed in Table 1 [26,27]. Thus Eq. (3) can be simplified as $d\rho/\rho = 4.5 \times 10^{-10} dp - 2.5 \times 10^{-4} dT$. From Ref. [21], the pressure change is $dp = \rho_0 c \omega A_0$, in which $\rho_0 c$ is the specific acoustic impedance of the acoustic medium, and ω and A_0 are the angular frequency and the amplitude of the vibration source, respectively. The density and the sound speed of water is about 1000 kg/m³ and 1500 m/s, respectively (see Appendix A). In the ultrasonic manipulation based on acoustic streaming [24], the maximum order of magnitude of ω and A_0 is 10⁷ rad/s and 10⁻⁶ m, respectively. Thus the order of magnitude of dp cannot be larger than 10⁷ Pa, and that of term $4.5 \times 10^{-10} dp$ is not larger than 10⁻³. In the acoustic streaming based manipulations, the temperature change in water at the manipulation point is usually less than 10 K. This means that the order of magnitude of term $2.5 \times 10^{-4} dT$ cannot be larger than 10⁻³. So the order of magnitude of $d\rho/\rho$ cannot be larger than 10⁻³ in the water, which means that the water density can be treated as constant for the ultrasonic manipulations based on acoustic streaming. For the acoustofluidic model in this work, the order of magnitude of parameters ω , A_0 and dT is less than the above stated maximum ones. Therefore, the water density can also be treated as constant in this work.

The steady acoustic streaming satisfies the following equation [4,22]:

$$\rho_0 (\bar{u}_i \partial \bar{u}_j / \partial x_i) = F_j - \partial \bar{p}_2 / \partial x_j + \eta \nabla^2 \bar{u}_j \quad (4)$$

where \bar{u}_i is acoustic streaming velocity, repeated suffix i and j represent x and y in the 2D model, ρ_0 is the fluid density in the undisturbed state ($\rho_0 = \rho|_{T=T_0}$, see Appendix A), F_j is the gradient of the Reynolds stress which acts on the fluid as a driving force of the acoustic streaming, and \bar{p}_2 is the time average of the 2nd order pressure or mean pressure. F_j is calculated by

¹ For interpretation of color in Fig. 1, the reader is referred to the web version of this article.

Table 1
Parameters of the acoustofluidic field.

Length of line vibration source L_s (m)	Width of acoustofluidic field W_a (m)	Length of acoustofluidic field L_a (m)
0.02	0.06	0.09
Frequency of line vibration source f (kHz)	Amplitude of line vibration source v (m/s)	Volume-to-shear viscosity ratio in water η'/η
20	$4\pi \times 10^{-3}$	2.1
Ratio of specific heats γ in water	Isothermal compressibility β_T (Pa $^{-1}$) in water at 298 K	Isobaric thermal expansion coefficient α_p (K $^{-1}$) in water at 298 K
1	4.5×10^{-10}	2.5×10^{-4}

$$F_j = -\partial(\overline{\rho_0 u_i u_j})/\partial x_i \quad (5)$$

where u_i is the vibration velocities in the sound wave, and the bar signifies the mean value over one period.

The total pressure P in the acoustic medium can be expanded into a Taylor series as follows [5]:

$$P = P_0 + \left(\frac{\partial p}{\partial \rho}\right)_{s,\rho=\rho_0} (\rho - \rho_0) + \left(\frac{\partial^2 p}{\partial \rho^2}\right)_{s,\rho=\rho_0} \frac{(\rho - \rho_0)^2}{2} + \dots \quad (6)$$

in which s means that the terms are evaluated in the isentropic state, and P_0 is the fluid pressure in the undisturbed state. The (1st order) sound pressure p_1 is

$$p_1 = \left(\frac{\partial p}{\partial \rho}\right)_{s,\rho=\rho_0} (\rho - \rho_0) = A \left(\frac{\rho - \rho_0}{\rho_0}\right) \quad (7)$$

where

$$A = \rho_0 \left(\frac{\partial p}{\partial \rho}\right)_{s,\rho=\rho_0} = \rho_0 c_0^2 \quad (8)$$

in which c_0 is the sound speed in the undisturbed state ($c_0 = c|_{T=T_0}$, see Appendix A). The 2nd order pressure p_2 is

$$p_2 = \left(\frac{\partial^2 p}{\partial \rho^2}\right)_{s,\rho=\rho_0} \frac{(\rho - \rho_0)^2}{2} = \frac{B}{2} \left(\frac{\rho - \rho_0}{\rho_0}\right)^2 \quad (9)$$

where

$$B = \rho_0^2 \left(\frac{\partial^2 p}{\partial \rho^2}\right)_{s,\rho=\rho_0} \quad (10)$$

From Eqs. (7) and (9), there is

$$p_2 = \frac{1}{2\rho_0 c_0^2} \frac{B}{A} p_1^2 \quad (11)$$

Therefore, the mean pressure \bar{p}_2 is calculated by

$$\bar{p}_2 = \frac{1}{2\rho_0 c_0^2} \frac{B}{A} \langle p_1^2 \rangle \quad (12)$$

where $\langle \rangle$ represents the time average over one period, and B/A is the nonlinear parameter of the acoustic medium, depending on the medium and temperature ($B/A = 5$ for water at 25 °C) [5,21]. The acoustic streaming also satisfies the continuity equation

$$\rho_0 \partial \bar{u}_i / \partial x_i = 0 \quad (13)$$

3. Results and discussion

Unless otherwise specified, the acoustic streaming field is computed when the acoustic medium's temperature T is 298 K, the operating frequency f is 20 kHz, and the amplitude of source vibration A_0 is 100 nm. In the calculation of the sound field and acoustic streaming, the relative tolerance of the solvers in the COMSOL Multiphysics software is 0.0001 and 0.001, respectively. Fig. 2a show us the distributions of the y -directional velocity of acoustic

streaming at $y = 0.04$ m, calculated by our finite element analysis method and by the analytical solution given in Appendix B and Ref. [22]. It is seen that the two acoustic streaming distributions are quite close at $y = 0.04$ m, which partially verifies our calculation method. Fig. 2b shows the computed sound pressure in the sound field, and Fig. 2c shows the computed acoustic streaming field. In Fig. 2c, the color denotes the magnitude of the acoustic streaming velocity, and the arrow denotes the direction and magnitude of the acoustic streaming velocity. In addition to the two main eddies EL (eddy on the left side) and ER (eddy on the right side) in the center of the field, which have been predicted by the traditional analytical solutions [5,23], a pair of additional circular eddies, denoted as ECL (eddy in the corner on the left side) and ECR (eddy in the corner on the right side), are found in the two corners of the field.

The effect of the sound field frequency on the pattern of acoustic streaming field is computed, and Fig. 3 shows patterns of the acoustic streaming field at 10 kHz, 40 kHz, 80 kHz and 216 kHz with the same velocity amplitude of the vibration source (1.26 cm/s). It is seen that as the frequency increases, the number of eddies of acoustic streaming increases, and the pattern becomes more complex. In the acoustic streaming field at 216 kHz, there are six eddies which have an orderly arrangement. It provides a method for manipulating small particles at several points simultaneously.

The acoustic streaming field was computed for different vibration source lengths L_s , and the result is shown in Fig. 4. Fig. 4a shows the acoustic streaming field for different lengths of the vibration source L_s . It indicates that as the vibration source length increases, eddies ECL and ECR in the two corners will disappear and the length of the main eddies will change. The acoustic streaming velocity has the maximum velocity at the boundary between eddies EL and ER. Fig. 4b shows the maximum velocity of the acoustic streaming versus the vibration source length. As the vibration source length increases, the maximum velocity increases and then decreases, and reaches the maximum when L_s/W_a is 2/3. The maximum velocity increase with L_s is because more acoustic energy is used to support the main eddies. The maximum velocity decrease with L_s is because a too long radiation line restrains the acoustic streaming from returning to the radiation boundary via the two sides.

The acoustic streaming field excited by two separated vibration line sources, was computed. In the computation, the vibration line sources are spatially symmetric about the y -axis, with identical vibration amplitude and frequency, and the total length of them is constant (0.02 m). Fig. 5a and b are the computed acoustic streaming field versus separation distance between the two vibration sources when the vibration sources are in and out of phase, respectively. Fig. 5a shows that the main eddy length decreases as the separation between the in-phase vibration sources increases, and increasing the separation can eliminate the two eddies in the corners. From a comparison between images a1 (in Fig. 5a) and b1 (in Fig. 5b), it is known that using out-of-phase vibration source can eliminate the two eddies in the corners.

Defining the phase of the left vibration source minus that of the right one as the phase difference, the acoustic streaming field versus the separation between the two vibration sources was

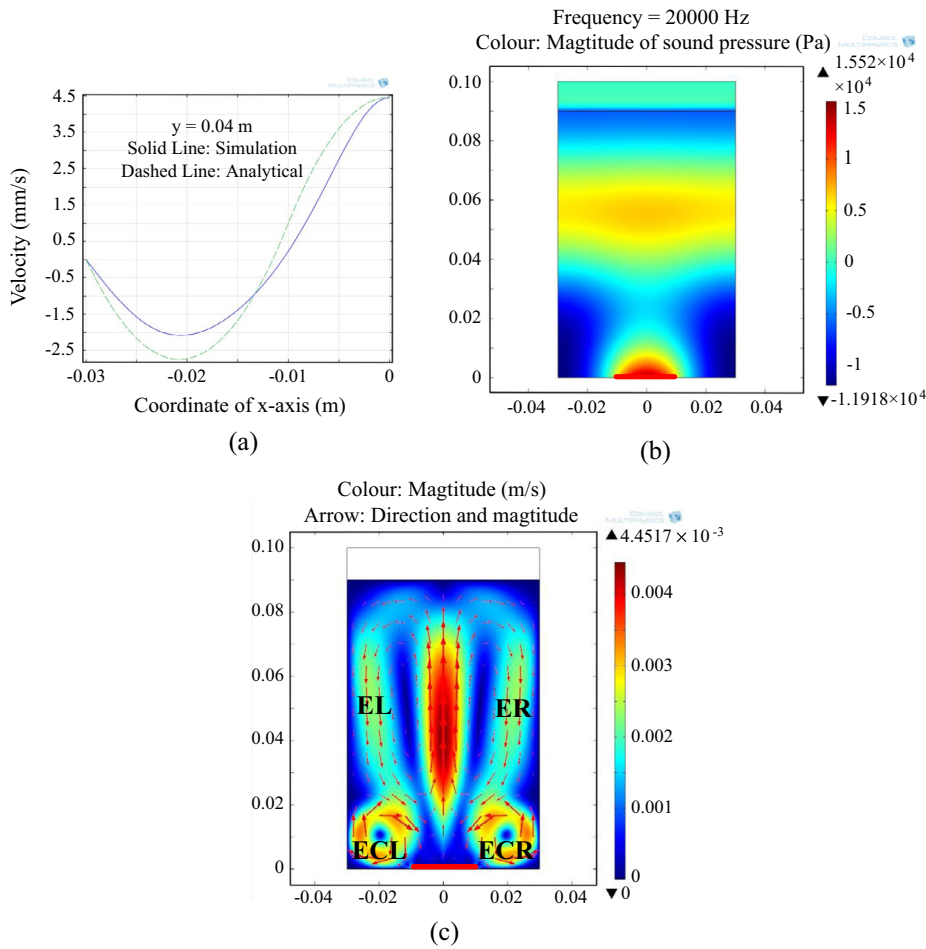


Fig. 2. Sound pressure and acoustic streaming field at $f = 20$ kHz, $A_0 = 0.1 \mu\text{m}$ and $T = 298$ K. (a) Distributions of the y -directional velocity at $y = 0.04$ m. (b) Pattern of sound pressure field. (c) Pattern of acoustic streaming field.

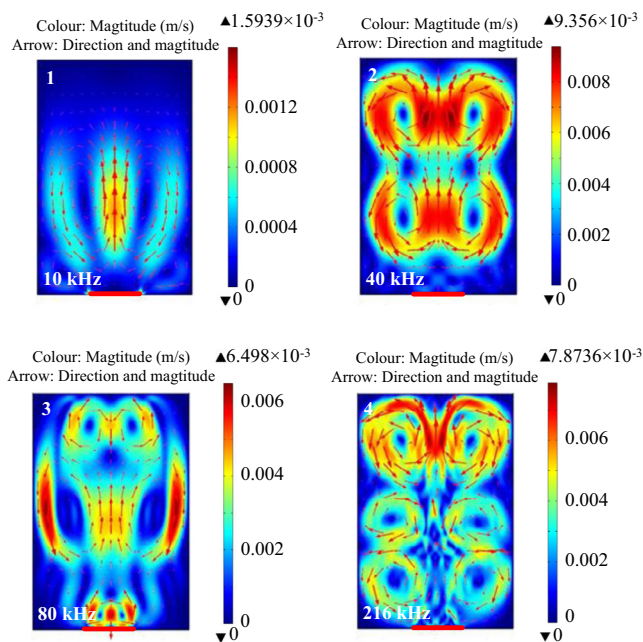


Fig. 3. Patterns of acoustic streaming field at different frequencies with constant velocity amplitude.

computed for the phase difference of $\pm\pi/2$, and the results are shown in Fig. 6. Unlike the acoustic streaming fields when the phase difference is 0 and π (see Fig. 5), the acoustic streaming fields are no more symmetric about the y -axis in this case. Also, it is seen that the acoustic streaming fields for the phase difference of $\pm\pi/2$ are reverse with each other, which means that a phase reversal of the vibration displacement or driving voltage of one of the vibration sources flips the acoustic streaming field's pattern.

The above theoretical results show the diversity in the acoustic streaming field's pattern, caused by the frequency, size, topology and phase distribution of its vibration source. The diversity indicates the possibility to implement new manipulating functions for micro/nano objects, such as concentrating and rotating micro/nano objects at multiple locations on a substrate simultaneously.

Investigating the effect of a micro/nano particle in acoustic field on the acoustic streaming becomes an important issue now that acoustic streaming has been employed in the ultrasonic micro/nano manipulations. The effect of a 0.5 mm-radius particle in the sound field on the acoustic streaming field was investigated by the FEM, and the results are shown in Fig. 7. In images a, b and c in Fig. 7, the particle is at (0 m, 0.05 m), (0.005 m, 0.05 m) and (0.01 m, 0.05 m), respectively. The relative coordinates of the particle (x/W_a , y/L_a) are (0, 5/9), (1/12, 5/9), (1/6, 5/9), respectively. By comparison with Fig. 2c, it is concluded that existence of the particle remarkably decreases the main eddy length when it is on the central axis, and an additional eddy will be generated when the particle is shifted from the central axis to a location other than the center of a main eddy.

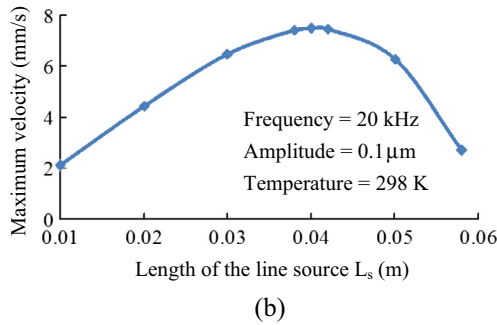
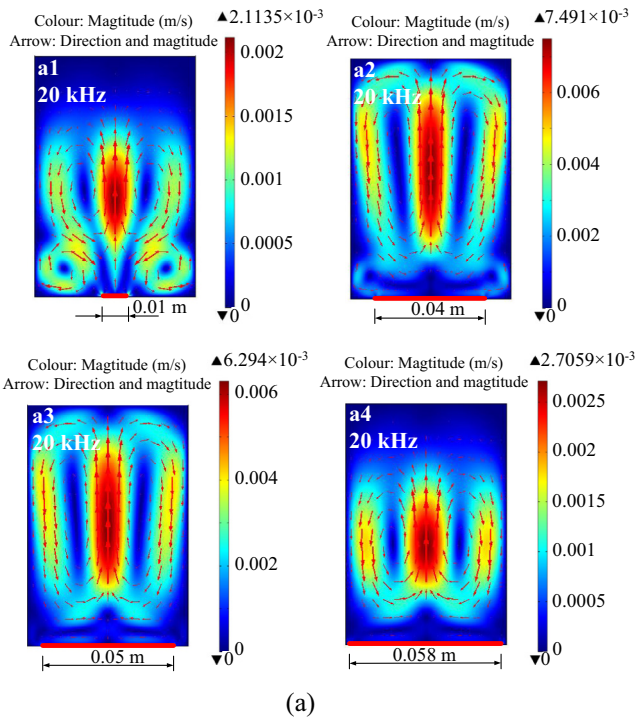


Fig. 4. (a) Patterns of acoustic streaming field at different lengths of the line vibration source. (b) Maximum velocity of the main eddies vs. the vibration source length.

Furthermore, the effect of the particle radius at (0, 0.05 m) on the acoustic streaming field was computed, and the results are shown in Fig. 8. The particle radius used in the calculation is 5 μm , 50 μm , 200 μm and 1000 μm . Fig. 8a indicates that as the particle becomes large, the main eddies become short while the size in the two corners has little change. Fig. 8b shows the acoustic streaming field length versus the particle radius when the particle is at (0, 0.05 m). In the measurement of acoustic streaming field length, the upper boundary of acoustic streaming field is defined by the location where the acoustic streaming velocity is 1/5 of the maximum value. It is seen that when the particle radius is larger than 200 μm (at 20 kHz), the acoustic streaming field length decreases little as the particle becomes large. Moreover, based on our computation, it is known that when the ratio of the particle radius to wavelength is less than 0.03%, the particle on the central axis has little effect on the acoustic streaming field.

Further analyses show that increasing the number of small particles in the acoustic field increases the number of the eddies, which is quite useful in some applications such as ultrasonic mixing. Fig. 8 also indicates that for a given acoustic field, the pattern and size of the eddies can be tuned by simply inserting a thin rod to a proper location in it.

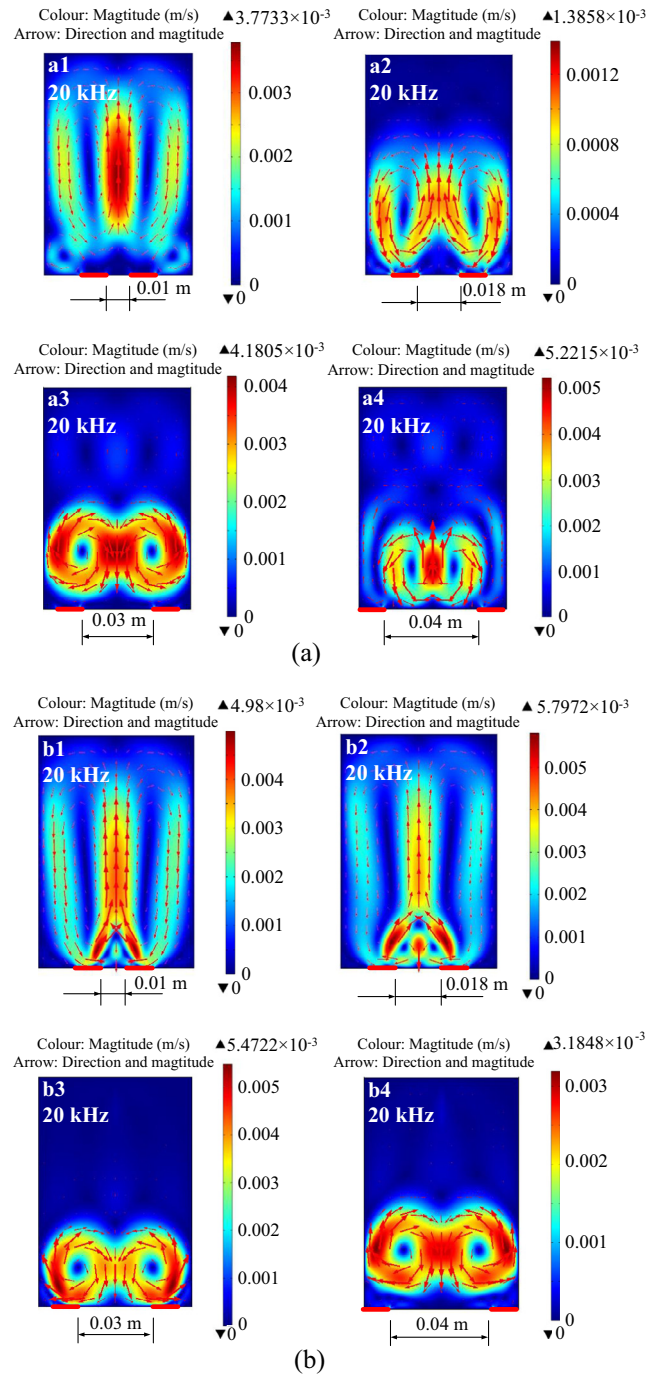


Fig. 5. Patterns of acoustic streaming field generated by two separated vibration sources with constant total length and symmetric spatial distribution about the central axis. (a) Vibration sources in phase. (b) Vibration sources out-of-phase by π .

The effect of temperature change of acoustic medium in an ultrasonic field was not understood before this work. For the model shown in Fig. 1, the effect of water temperature on the acoustic streaming field was investigated, and the results are shown in Figs. 9 and 10. In the computation, formulas describing the temperature dependence of the sound speed, density, heat capacity at constant pressure and volume, thermal conductivity, and shear viscosity of water at 1 atm, given by COMSOL Multiphysics software, were utilized (see Appendix A for the details).

Fig. 9 shows the pattern of the acoustic streaming field in water at temperature $T = 274 \text{ K}$, 318 K, and 372 K, which indicates that

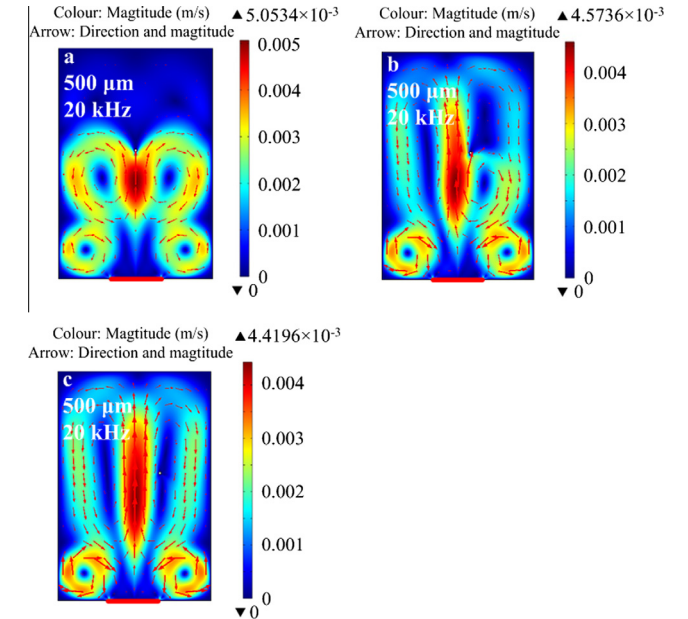
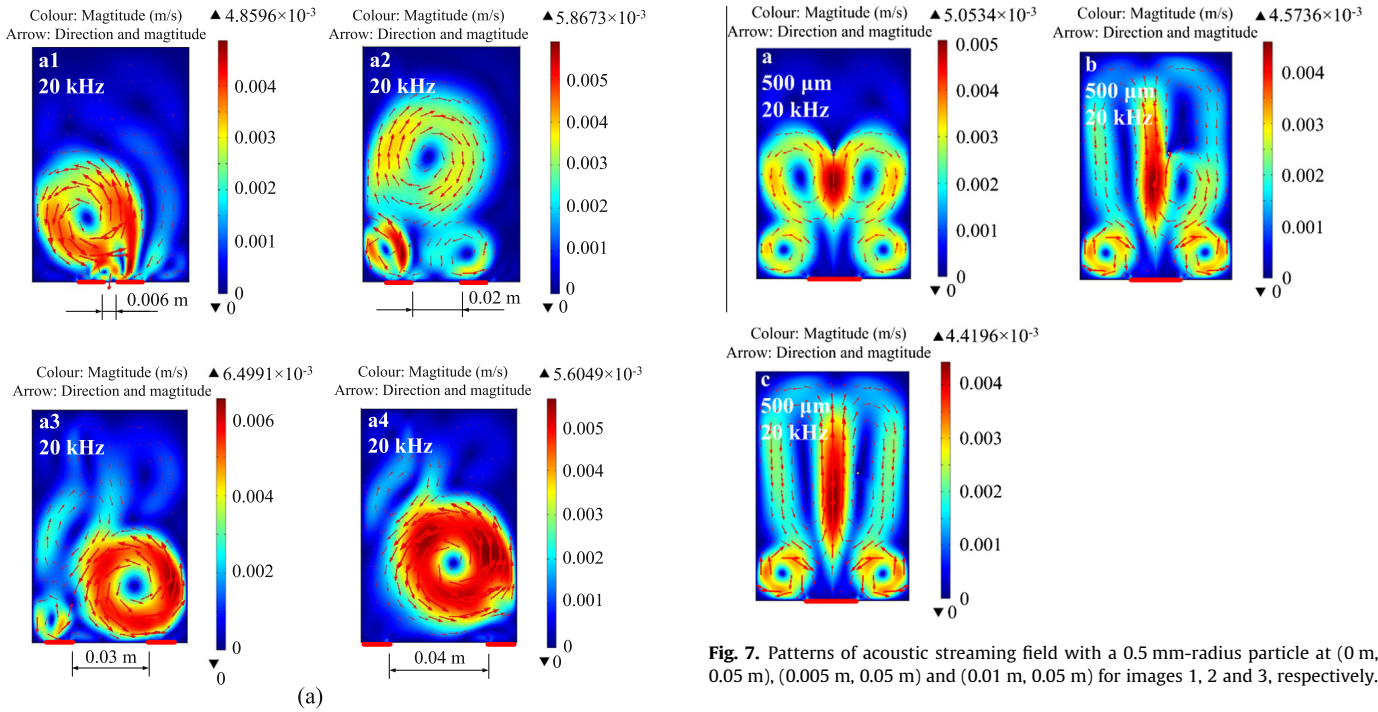


Fig. 7. Patterns of acoustic streaming field with a 0.5 mm-radius particle at (0 m, 0.05 m), (0.005 m, 0.05 m) and (0.01 m, 0.05 m) for images 1, 2 and 3, respectively.

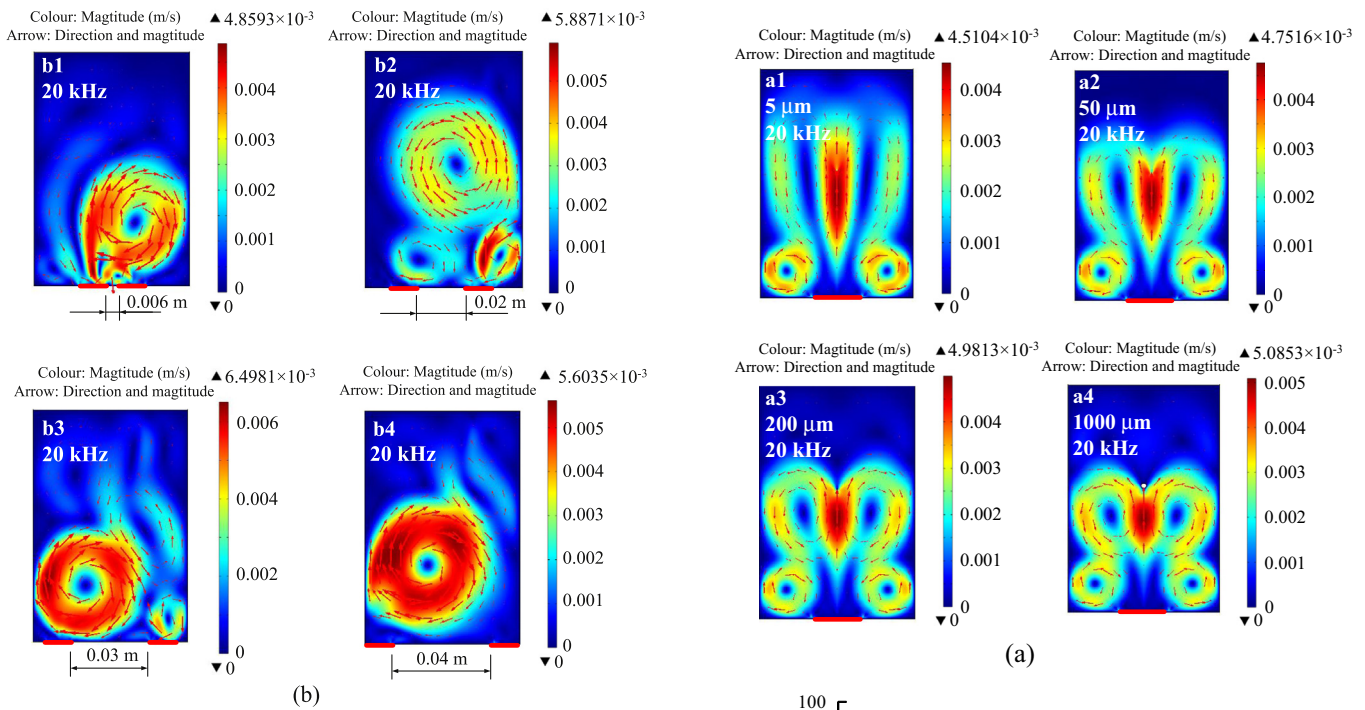


Fig. 6. Patterns of acoustic streaming field generated by two separated vibration sources with constant total length and symmetric spatial distribution about the central axis. (a) $-\pi/2$ vibration phase difference. (b) $\pi/2$ vibration phase difference.

when the water temperature increases, the length of the main eddies increases and the flowing pattern has little change. Fig. 10a gives the maximum velocity of the main eddies versus the temperature. It shows that as the temperature increases, the velocity decreases first and then increases. In the temperature range from 1 °C to 99 °C, the acoustic streaming velocity has a fluctuation of 17%, and reaches the minimum at about 60 °C. Fig. 10b shows the calculated angular velocity of the corner eddies versus the temperature. As the temperature increases, the angular velocity increases.

Fig. 8. The effect of the size of a particle at (0 m, 0.05 m) on the acoustic streaming field. (a) Patterns of acoustic streaming field for different particle radii. (b) The length of the acoustic streaming field versus particle radius.

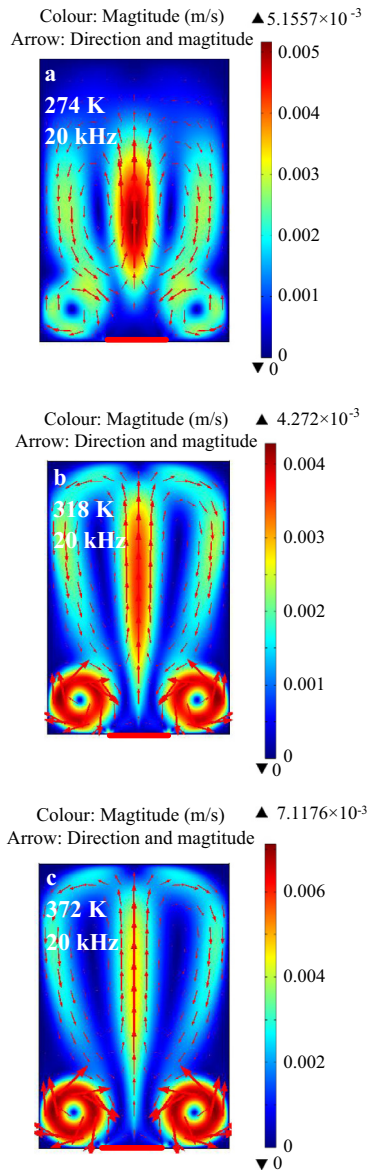


Fig. 9. The acoustic streaming field's patterns in water at different temperatures.

For the convenience of analyzing Figs. 9 and 10, values of sound speed c , density ρ , shearing viscosity η and acoustic dissipation factor b of water at different temperatures are listed in Table 2. It is seen that as the temperature changes from 274 K to 372 K, the acoustic dissipation factor b decreases monotonously. Thus as the temperature rises, the sound wave can transmit further, which results in longer main eddies, as shown in Fig. 9.

From Table 2, it is also seen that as the temperature increases from 274 K to 332 K, the acoustic dissipation factor b decreases. This causes a decrease of the spatial gradient of Reynolds stress and of the maximum velocity of the main eddies, as shown in Fig. 10a. As the temperature increases from 274 K to 332 K, the decrease of the acoustic dissipation factor b is not very remarkable, and neither is the spatial gradient of the Reynolds stress. However, in this temperature range, the shear viscosity decreases as the temperature increases. This results in an increase of the maximum velocity of the main eddies, as shown in Fig. 10a. The increase of angular velocity of the corner eddies with the temperature increase, as shown in Fig. 10b, is caused by the decrease of the shear viscosity. From Fig. 10b, it is also seen that the curve's slope

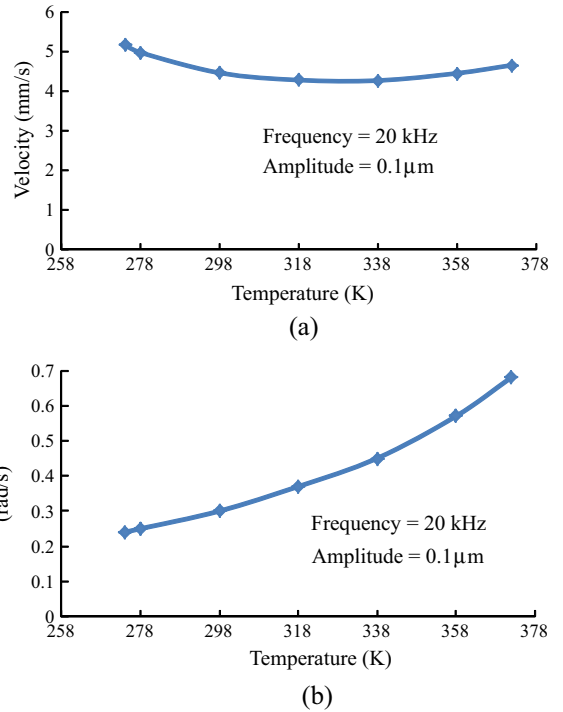


Fig. 10. The acoustic streaming field's velocity in water at different temperatures. (a) Maximum velocity of the main eddies vs. temperature. (b) Angular velocity of the corner eddies vs. temperature.

Table 2

Sound speed, density, shear viscosity and acoustic dissipation factor of water at different temperatures.

T (K)	274	298	332	353	372
c (m/s)	1408.7	1494.3	1549.9	1554.2	1543.6
ρ (kg/m ³)	1003.8	998.2	985.1	974.0	961.9
η (Pa s)	0.00174	0.00089	0.00048	0.00036	0.00028
b (Pa s)	0.00599	0.00308	0.00164	0.00124	0.00098

in the temperature range from 274 K to 332 K is less than that from 332 K to 372 K. This is because the acoustic dissipation factor b decreases faster with the temperature rise in the range from 274 K to 332 K than in the range from 332 K to 372 K (see Table 2).

4. Conclusions

In summary, for a 2D rectangular acoustofluidic field with a traveling wave and using water, a diversity of acoustic streaming is exhibited with the change of the working frequency, vibration excitation source length, and distance and phase difference between two separated symmetric vibration excitation sources. It is also found that the existence of micro particles has more or less influence on the distribution of acoustic streaming, depending on its position and size. In addition, the computation results show that with increase of the acoustic medium's temperature, the speed of the main acoustic streaming decreases first and then increases, and the angular velocity of the corner eddies increase monotonously. These conclusions provide useful guidelines for controlling the acoustic streaming field in nano manipulations.

Acknowledgements

This work is supported by the following funding organizations in China: National Science Foundation of China (No. 91123020),

State Key lab of Mechanics and Control of Mechanical Structures (MCMS-0313G01 and MCMS-0314G01), Nanjing University of Aeronautics and Astronautics (No. S0896-013), the “111” project (No. B12021), and PAPD.

Appendix A

All functions in this appendix are from the COMSOL Multiphysics software.

Temperature dependence of physical properties of water

$$\text{Speed of sound } c(\text{m/s}) = 9.3009 \times 10^{-5} \times T^3 - 0.1174 \times T^2 + 47.8834 \times T - 4.8107 \times 10^3$$

$$\text{Density } \rho(\text{kg/m}^3) = 3.71822313 \times 10^{-7} \times T^3 - 0.0030112376 \times T^2 + 1.40050603 \times T + 838.466135$$

Heat capacity at constant pressure $C_p(\text{J}/(\text{kg K}))$

$$= 3.62536437 \times 10^{-7} \times T^4 - 5.38186884 \times 10^{-4} \times T^3 + 0.309866854 \times T^2 - 80.4072879 \times T + 12010.1471$$

Heat capacity at constant volume $C_v(\text{J}/(\text{kg K})) = C_p/\gamma$, in which γ does not depend on the temperature.

Thermal conductivity $k_r(\text{W}/(\text{m K}))$

$$= 7.97543259 \times 10^{-9} \times T^3 - 1.58366345 \times 10^{-5} \times T^2 + 0.00894880345 \times T - 0.869083936$$

Shear viscosity $\eta(\text{Pa s}) = 3.8457331488 \times 10^{-16} \times T^6$

$$- 9.0790692686 \times 10^{-13} \times T^5 + 8.9042735735 \times 10^{-10} \times T^4 - 4.6454090319 \times 10^{-7} \times T^3 + 1.3604562827 \times 10^{-4} \times T^2 - 0.021224019151 \times T + 1.3799566804$$

Appendix B

For the acoustofluidic field model in this work, Ref. [22] has given the analytical solution of the acoustic streaming velocity in the axial direction:

$$u_y = B_0(h - 2z_1) \left(x + \frac{h}{2}\right) + (2\mu)^{-1} K \left(x + \frac{h}{2}\right) \left(x - \frac{h}{2}\right) \quad \text{for } -\frac{h}{2} \leq x \leq -\frac{h}{2} + z_1$$

$$u_y = B_0 \left[h \left(x + \frac{h}{2}\right) - \left(x + \frac{h}{2}\right)^2 - z_1^2 \right] + (2\mu)^{-1} K \left(x + \frac{h}{2}\right) \left(x - \frac{h}{2}\right) \quad \text{for } -\frac{h}{2} + z_1 < x \leq 0$$
(A1)

in which μ is the shearing viscosity of the acoustic medium, h is the width of the acoustofluidic field, z_1 is the distance between a corner at the bottom of the acoustofluidic field and the vibration excitation source, and parameters B_0 and K are

$$B_0 = \frac{\rho_0 \alpha A_0^2}{2\mu} \quad (A2)$$

$$K = \mu B_0 \left[2 - 3 \left(\frac{2z_1}{h}\right)^2 + \left(\frac{2z_1}{h}\right)^2 \right] \quad (A3)$$

where ρ_0 is the fluid density, α is an absorption coefficient, and A_0 is the velocity amplitude of the vibration source. The hypotheses used

in the derivation include: (i) the flow of acoustic streaming is continuous, and (ii) the boundary is no-slip. These hypothesis are the same as the ones used in our work.

When the acoustofluidic field has a width of 0.06 m ($h = W_a = 0.06$ m), and the distance between a corner at the bottom of the acoustofluidic field and the vibration source is 0.02 m ($z_1 = (W_a - L_s)/2 = 0.02$ m), the solution is

$$u_y = \frac{871}{27}(x+0.03)^2 - \frac{134}{225}(x+0.03) \quad \text{for } -0.03 \leq x \leq -0.01(\text{m})$$

$$u_y = -\frac{938}{27}(x+0.03)^2 + \frac{469}{225}(x+0.03) - \frac{67}{2500} \quad \text{for } -0.01 < x \leq 0(\text{m})$$
(A4)

Eq. (A4) is used in the calculation for Fig. 2a in this paper.

References

- [1] C. Eckart, Vortices and streams caused by sound waves, *Phys. Rev.* 73 (1948) 68–76.
- [2] W.L. Nyborg, Acoustic streaming due to attenuated plane waves, *J. Acoust. Soc. Am.* 25 (1953) 68.
- [3] P.J. Westervelt, The theory of steady irrotational flow generated by a sound field, *J. Acoust. Soc. Am.* 25 (1953) 60.
- [4] J. Lighthill, Acoustic streaming, *J. Sound Vib.* 61 (1978) 391–418.
- [5] Oleg V. Abramov, High-Intensity Ultrasonics: Theory and Industrial Applications, Gordon and Breach Science Publishers, 1998.
- [6] J. Hu, K. Nakamura, S. Ueha, Optimum operation conditions of an ultrasonic motor driving fluid directly, *Jpn. J. Appl. Phys.* 35 (1996) 3289–3294.
- [7] J. Hu, K. Cha, K. Lim, New type of linear ultrasonic actuator based on a plate-shaped vibrator with triangular grooves (Letter), *IEEE Trans. Ultrason. Ferroelectr. Freq. Control* 51 (2004) 1206–1208.
- [8] J. Hu, A. Santoso, A π -shaped ultrasonic tweezers concept for manipulation of small particles, *IEEE Trans. Ultrason. Ferroelectr. Freq. Control* 51 (2004) 1499–1507.
- [9] A.L. Bernassau, P. Glynne-Jones, F. Gesellchen, M. Riehle, M. Hill, D.R.S. Cumming, Controlling acoustic streaming in an ultrasonic heptagonal tweezers with application to cell manipulation, *Ultrasonics* 54 (2014) 268–274.
- [10] N. Li, J. Hu, H. Li, S. Bhuyan, Y. Zhou, Mobile acoustic streaming based trapping and 3-dimensional transfer of a single nanowire, *Appl. Phys. Lett.* 101 (2012).
- [11] H. Li, J. Hu, Noncontact manipulations of a single nanowire using an ultrasonic micro-beak, *IEEE Trans. Nanotechnol.*, doi: 10.1109/TNANO.2013.2278703.
- [12] N. Li, J. Hu, Sound controlled rotary driving of a single nanowire, *IEEE Trans. Nanotechnol.*, doi: 10.1109/TNANO.2013.2277731.
- [13] Y. Zhou, J. Hu, S. Bhuyan, Manipulations of silver nanowires in a droplet on low-frequency ultrasonic stage, *IEEE Trans. Ultrason. Ferroelectr. Freq. Control* 60 (2013) 622–629.
- [14] O.V. Rudenko, A.P. Sarvazyan, S.Y. Emelianov, Acoustic radiation force and streaming induced by focused nonlinear ultrasound in a dissipative medium, *J. Acoust. Soc. Am.* 99 (1996) 2791.
- [15] N. Riley, Acoustic streaming, *Theoret. Comput. Fluid Dynam.* 10 (1998) 349–356. 10.
- [16] C. Bradley, Acoustic streaming field structure. Part II. Examples that include boundary-driven flow, *J. Acoust. Soc. Am.* 131 (1) (2012) 13–23.
- [17] T. Kamakura, K. Matsuda, Y. Kumamoto, Acoustic streaming induced in forced Gaussian beams, *J. Acoust. Soc. Am.* 97 (1995) 2740.
- [18] T. Kamakura, T. Sudo, K. Matsuda, Y. Kumamoto, Time evolution of acoustic streaming from a planar ultrasound source, *J. Acoust. Soc. Am.* 100 (1996) 132.
- [19] Y. Wada, D. Koyama, K. Nakamura, Finite element analysis of acoustic streaming from a planar ultrasound source, *Japanese J. Appl. Phys.* 49 (2010) 07HE15.
- [20] L.N. Liebermann, The second viscosity of liquids, *Phys. Rev.* 75 (1949) 1415–1422.
- [21] Lawrence E. Kinsler, Austin R. Frey, Alan B. Coppens, James V. Sanders, *Fundamentals of Acoustics*, Hamilton Press, 1999.
- [22] W.L. Nyborg, Acoustic streaming, in: W.P. Mason (Ed.), *Physical Acoustics*, vol. 2B, Academic, New York, 1965, pp. 265–331.
- [23] D. Möller, T. Hilsdorf, J.T. Wang, J. Dual, Acoustic streaming used to move particles in a circular flow in a plastic chamber, *AIP Conf. Proc.* 1433 (2012) 775–778.
- [24] J. Hu, *Ultrasonic Micro/Nano Manipulations: Principles and Examples*, World Scientific, 2014.
- [25] P.B. Muller, R. Barnkob, M.J.H. Jensen, H. Bruus, A numerical study of microparticle acoustophoresis driven by acoustic radiation forces and streaming-induced drag forces, *Lab Chip.* 12 (2012) 4617–4627.
- [26] F. Corsetti, E. Artacho, J.M. Soler, S.S. Alexandre, M.-V. Fernández-Serra, Room temperature compressibility and diffusivity of liquid water from first principles, *J. Chem. Phys.* 139 (2013) 194502.
- [27] F. Mallamace, C. Corsaro, D. Mallamace, S. Vasi, C. Vasi, H.E. Stanley, Thermodynamic properties of bulk and confined water, *J. Chem. Phys.* 141 (2014) 18C504.